Mechanisms and processes of pulsed laser ablation in liquids during nanoparticle production

M. Dell'Aglio[a], R. Gaudiuso[a], O. De Pascale[a], A. De Giacomo[b,a,*]

[a] CNR-IMIP sec Bari, Via Amendola 122/D, 70126 Bari, Italy

[b]Chemistry Department, University of Bari, Via Orabona 4, 70126 Bari, Italy

* E-mail: alessandro.degiacomo@imip.cnr.it; Fax: +39 080 5929520;Tel: +39 080 5929511, Chemistry Department, University of Bari, 70126, Bari, Italy.

Highlights:

Determination of plasma features

NPs formation by PLAL

Cavitation bubble dynamics and mechanisms of NP release in liquids

Abstract:

In the last decade Pulsed Laser Ablation in Liquids (PLAL) has been widely investigated from the fundamental point of view, and various theories have been proposed. Although many important achievements have been obtained by the scientific community, many aspects still need to be clarified and many contradictions arise when comparing the interpretation of similar experiments carried out by different authors. In this paper we have reconsidered previous works focused on specific processes and stages of the PLAL, in order to outline a modern and comprehensive point of view of the overall physical aspects of PLAL. With this aim, several simultaneous diagnostic methods have been applied during the production of metallic nanoparticles (NPs), i.e. optical emission spectroscopy and fast imaging for the investigation of the laser-induced plasma, shadowgraph for the study of the cavitation bubble, and Double Pulse Laser Ablation in Liquid (DP-LAL) and laser scattering for the investigation of NPs location and mechanisms of release in solution. The connection between the various stages of the DP-LAL allows understanding the main characteristics of the produced NPs and the typical timescales of the basic mechanisms involved in PLAL.

Keywords: NPs, laser ablation in liquids, laser induced plasma, laser induced bubble

1. Introduction

The great effort that the scientific community has put in the last decade in the study of nanoscience and nanotechnology has been leading the research toward the development of new methodologies of nanostructures synthesis. Among them, Pulsed Laser Ablation in Liquid, PLAL, is gaining an increasing interest thanks to several promising advantages, which include: environmental sustainability, easy experimental set-up (which does not require extreme conditions of the ambient of synthesis), long-lasting stability of the nanoparticles, which are produced completely free of undesired contaminants or dangerous synthesis reactants. The increase of the research products in this field and in the period 1998-2011 has been already analyzed in [1, 2] , and until now their number has continued to grow. The nanomaterials and nanostructures that can be produced are extremely varied, as well as their applications. Refs. [3- 5] present the most significant papers relative to the different typologies of nanostructures produced by PLAL with some of their applications, and focus on physical and chemical fundamentals of PLAL.

Precisely because of this great interest for PLAL nanostructures fabrication, studying the mechanisms of formation is extremely interesting in order to improve the fundamental understanding in this field. Until now, important goals have been reached, especially in the last decade, but much still needs to be clarified. In particular, the laser induced plasma and cavitation bubble dynamics during the laser ablation in liquids play crucial roles. In previous studies [6, 7] we combined complementary optical techniques with high temporal resolution and investigated in details the roles of the laser-induced shockwave and plasma in the early time of these processes, as well as the connections between the cavitation bubble formation and dynamics and the formation of NPs [8, 9, 10]. On the other hand, theoretical studies were also carried out on the mechanisms of NPs formation [11, 12]. This paper is based on some fundamental experiments, and its aim is to give and discuss a modern and comprehensive point of view on the mechanisms and the processes involved in the PLAL technique.

2. Experimental investigation of the processes involved in the production of NPs by PLAL.

Laser induced breakdown of submerged targets is characterized by visible plasma emission and the production of shock waves and of cavitation bubbles. The duration of each of these processes is sketched in Fig.1: after laser-matter interaction, laser-induced breakdown occurs, followed by the shock wave formation, plasma expansion and cooling, and by cavitation bubble formation, expansion and collapse. Upon the bubble collapse, the nanoparticles, which are produced during the

plasma cooling phase, can diffuse in the surrounding liquid and form a colloidal solution. Investigation of this series of processes is challenging because it requires different diagnostic techniques operating simultaneously. Moreover the dimension of the systems to investigate, i.e. the laser-induced plasma and the produced nanomaterial, requires detection methods with high sensitivity and high temporal resolution. In the frame of these considerations, we employed four different techniques for the experiments presented in this review: optical emission spectroscopy for the investigation of the laser-induced plasma [13], fast shadowgraph [14, 6] for the measurement of the cavitation bubble dynamics, laser scattering [6, 15, 16] and Double Pulse-LAL (DP-LAL) [7] to monitor the laser-induced breakdown and the produced nanoparticles. Other techniques that can be used for this aim include, for example, laser induced fluorescence and X-ray scattering [8, 9]. In order to better display some characteristics of the processes, targets with different geometry were employed to describe the phenomena involved in PLAL. In particular, in addition to the typical bulk targets (most usually disks or parallelepipeds of some mm of thickness), wire-shaped targets of hundreds of microns of diameter were used too. The main advantage of the latter target geometry, as already discussed in details in [6, 17], is that it allows a larger field of view for the detection. Finally in this paper we analyze the mechanisms and the processes occurring during PLAL with a laser pulse with duration of few nanoseconds (6 ns) and irradiance > 1 GW cm^{-2}.

2.1 Plasma production and cooling.

When laser pulses with irradiance between 0.1-1 GW cm^{-2} interact with a solid target, seed electrons are ejected from the target by multiphoton ionization and then, as a consequence of the photon absorption by inverse Bremsstrahlung, the ablated particles form a hot atomic plasma [18]. When ablation occurs, the number density of the irradiated material can be expected to change with a continuous trend during the solid-to-gas phase transition. This means that initially a very dense and hot plasma is formed, so that instantaneous expansion occurs. The plasma expands supersonically driving a shock wave in the surrounding environment, and then it slows down compressing the surrounding liquid until the plasma itself extinguishes. The main elementary processes that sustain the plasma induced in a liquid environment are essentially the same that occur during ablation in air [19, 20], the main differences being due to the different competition between the elementary processes and the different degree of energy exchange with the surrounding environment. Because of the low compressibility of the liquid, the plasma is suddenly confined so that it holds a density in the order of 10^{20} cm^{-3} and an ionization degree close to unity. At these

conditions atoms and ions in the plasma phase are affected by the Debye-Hückel effect so that most excited levels are not allowed and radiative recombination is the predominant process [19, 21].
Indeed upon 0.1-1 GW cm^{-2} laser ablation, the plasma is characterized by high-density effects [22] and, as a consequence of the limitation in the number of allowed excited levels, excitation and de-excitation by electron impact are replaced by ionization and recombination. In this scenario, the typical discrete spectrum, that reflects the Boltzmann distribution of atoms and ions , cannot be for the most of plasma evolution. Moreover, as a consequence of the recombining character of the laser induced plasma, radiative recombination becomes extremely efficient and is the main cause of deviation from the Local Thermal Equilibrium (LTE) condition, as discussed in details in [23].
The main effect of the predominance of radiative recombination on the other mechanisms is that the plasma emission spectrum is characterized by a continuum radiation. Since in the experimental conditions discussed in this work the plasma spectrum in liquid is a broad continuum that resembles a Planck-like distribution (though conceptually it is not a black body radiation) , it can be used to determine the temperature of the plasma by applying the "Planck plot" method described in [24]. In previous studies [6, 16], the temperature of a laser-induced plasma in water was found to be in the range 4000-6000 K. In addition to determining the plasma parameters, in the case of NP production it is very interesting to study the evolution of the plasma volume, which can be successfully done by fast imaging techniques. As an example Fig.2 shows a fast-camera image coupled with shadowgraph, acquired during PLAL of a Pt wire, which qualitatively displays the behaviour of the volume of the luminous plasma during the plasma persistence time. In this experiment it is evident that the plasma cooling is extremely fast, decreasing the size of the plasma and inducing vaporization of the surrounding medium at the front head of the plasma itself.
The plasma cooling process can be studied by time-resolved emission spectroscopy and fast imaging [25] in order to estimate when the NPs formation process starts. For example, Fig. 3 reports the temporal evolution of emission intensity and of plasma temperature as determined by Planck plot analysis during metal ablation under water (Ti and Cu bulk targets immersed in water). These data reveal two important features of the plasma cooling process: 1) the plasma emission intensity increases very fast and then exponentially decreases until the plasma extinguishes; 2) on the contrary, the plasma temperature holds a more or less constant value throughout most of the plasma persistence time , i.e. 500 ns. Later on it is not possible to measure the electronic temperature because the emission signal is too low and the spectral bands due the molecular recombination at the border of the plasma are the predominant emission signal [26]. The images taken with a fast camera and reported in Fig. 2 show that the plasma cooling proceeds from the front head to the interior, and we can suppose that during this process the plasma core keeps its

internal energy, at least in the initial part of the cooling process (500 ns), when most of the ablated mass undergoes phenomena responsible for NPs formation. In other words the plasma is cooling down shell by shell, starting from the external ones, and the total amount of emitting species decreases because atoms aggregate to generate the nanoparticles and are thus subtracted from the collisional plasma. Moreover, since the plasma core holds the same temperature throughout its persistence time, the cooling process occurs in constant thermodynamic conditions and, whatever the mechanism of formation, the produced nanoparticles are generated with very similar size and shape, which depend on the experimental conditions [27].

Finally, as a consequence of the high thermal capacity of the surrounding liquid, the energy exchange between the plasma itself and the adjacent compressed liquid layer proceeds extremely fast. Thus, the ablated material in the plasma cools down, at first by reducing ions to neutral species by recombination and then by producing the nanoparticles, which occurs almost immediately, within the first tens of nanoseconds after the laser pulse, until the complete extinction of the plasma.

2.2 Cavitation bubble evolution.

In the previous section we focused on the plasma cooling process promoted by the fast release of energy from the plasma to the surrounding liquid. Due to this transfer of energy, the liquid at the contact zone with the plasma front undergoes a phase transition that causes the formation of a thin layer of vapour around the plasma volume [28 - 36]. The thin water vapour layer can be clearly seen in Fig.2 as a dark zone around the plasma, due to the change of the refractive index caused by the high vapour pressure making the medium opaque. This vapour layer is the early cavitation bubble. The vapour layer forms at high temperature and, due to its high pressure, it expands in all directions, both against the liquid, thus generating the cavitation bubble, and against the plasma, thus causing the plasma confinement (Fig.1). The cavitation bubble radius can be estimated by fast shadowgraph, and the temperature and the pressure of the vapour inside the bubble can be determined with the Van der Waals state equation, as described in details in [6]. Fig 4a and b show the typical bubble dynamics in liquid environment when a laser is focused on a wire and on a bulk target, respectively. The bubble lifetime is usually in the order of hundreds of microseconds, i.e. 2 orders of magnitude longer than the duration of the plasma itself, and depends strongly on laser pulse characteristics such as wavelength, output energy and focusing condition, pulse duration, external pressure [37]. The bubble dynamics comprises an expansion stage and a subsequent compression stage, which can be repeated several times like a damping oscillator [20]. Between the

expansion and the compression stages, when the pressure inside the bubble reaches the saturation pressure at the liquid temperature, the bubble equilibrates with the surrounding liquid. In this condition, the bubble reaches the maximum radius and persists in this quasi-equilibrium status longer than it does in the compression and collapse stages, so that the produced NPs have longer time and a larger volume to diffuse, thus decreasing their local concentration. Fig 5 shows three frames of a time-resolved shadowgraph (a) and scattering images (b) obtained in the case of wire-shaped and bulk targets. These frames were chosen so to give examples of the early expansion, of the maximum expansion and of the collapse of the cavitation bubble.

Pressure and temperature in the bubble can be calculated by experimentally determining the bubble radius from the fast shadowgraph images [6] and by applying the Van der Waals equation. Table 1 lists the values obtained with this method at different times of the bubble evolution, which show that during the expansion and collapse phases both temperature and pressure change very fast, while near the maximum of the expansion only moderate changes occur.

2.3 Nanoparticle diffusion in the cavitation bubble and release in solution.

As the bubble forms at the plasma front, the produced material is sucked inside the cavitation volume during the bubble expansion, and then it diffuses inside the bubble. The initial rate of bubble expansion is much higher than the diffusion rate of nanoparticles, thus most material is contained inside the bubble. At the maximum of its expansion, the bubble volume is about two orders of magnitude larger than at the beginning of its evolution (i.e. right after the plasma cooling is complete). Consequently, in this condition of maximum expansion the local concentration of NPs in the bubble is the minimum throughout the whole bubble evolution. After the maximum expansion stage, the bubble starts to progressively shrink, and the radius changes with the same rate as during the expansion (but of course it decreases instead of increasing). During the collapse stage, the NPs that were filling the whole bubble volume are now pushed against the target, following the vapour stream, and thus accumulate at the bubble boundary. This is shown in Fig.5 (in particular in the collapse stage images) which compares the shadowgraph and the scattering images, and it has also been observed in small angle X-ray scattering experiments, reported in [9]. Moreover, the formed NPs act like a cloud of gas particles, but obviously they have higher density than the water vapour and are partially charged, thus resulting less compressible than the water vapour. Thus at the end of the collapse stage, when the bubble is sharply decreasing its volume, they occupy a larger volume than the bubble itself. This implies that the compressed vapour bubble is not able to drag

nanoparticles while shrinking towards the target and passing through the cloud of NPs, thus the NPs themselves are released in the liquid, as shown schematically in fig 6.

Studying the distribution of NPs in the bubble is rather difficult from the experimental point of view because at high pressure the bubble is opaque and the laser scattering technique is not sensitive enough. Recently small angle X-ray scattering has been employed for studying the formation of Au-NPs and their distribution inside the cavitation bubble [9]. These experiments have shown that, in agreement with the proposed description, most NPs contained in the bubble are close to the target, due to the slower drift velocity with respect to the front head of the bubble vapour. A simpler way to check qualitatively the location of the NPs in the bubble is to shoot a second laser pulse focussed inside the bubble volume in order to produce a secondary plasma from the material ablated by the first pulse. In this case, changing the interpulse delay between the first ablation pulse and the second one, it is possible to probe the ablated material inside the bubble by inducing the material breakdown, and to image the position of the plasma. The energy of the second pulse partly induces the breakdown of the ablated material and partly reaches the target surface generating a new ablation. The amount of laser pulse energy that reaches the target depends on the concentration of NPs in the focal volume. This experimental technique has been already applied for controlling the particle size and concentration during DP-LAL (Double Pulse – Laser Ablation in Liquid) [7] and can be efficiently used with the described approach, also as a diagnostic tool for understanding the distribution of NPs in the bubble volume. Fig. 7 shows different shadowgraphs of the plasma induced by the second pulse, taken at different time delay after the first ablation pulse. The temporal trend of the bubble radius (as obtained from the shadowgraphs) is reported for highlighting the bubble condition at which the second probing laser pulse is shot. Fig.7 indicates that the plasma has two components: one close to the border of the bubble due to the NP breakdown and one close to the target due to the secondary ablation of the target itself. During the bubble expansion phase, as the volume of the bubble is small and the NPs are in front of the target, most energy of the second laser pulse is spent in the NP breakdown , thus the second laser pulse generates an extended and luminous plasma in the interior of the bubble and only a minor plasma directly on the target surface. On the contrary, when the bubble is in equilibrium with the surrounding environment, its volume is larger and, as discussed in the previous section, this stage lasts comparatively longer than any stages of the bubble expansion and collapse, thus the particles have enough time to diffuse inside the bubble volume and strongly decrease their local concentration. The result is that in this situation NPs are not concentrated enough as to undergo the breakdown from the second laser pulse, which therefore deposits most of its energy on the target surface, generating a secondary ablation and a secondary plasma located mainly at the target surface. During the bubble shrinking phase the

situation is similar to that described in the early expansion phase. Finally, after the bubble collapses (200 μs) NPs are released in water in front of the target, thus the second laser pulse is shielded and prevented from reaching the target, producing the breakdown at the position where the NP cloud is placed. Thanks to the increase of concentration during the collapse phase, the NP release can be detected also with laser scattering, as shown in Fig.5 in the case of ablation of bulk and wire-shaped targets.

3. Conclusions

In this paper the fundamental processes occurring during PLAL (Pulsed Laser Ablation in Liquid) for NPs formation were studied by applying different time-resolved diagnostic techniques, i.e. optical emission spectroscopy, shadowgraph, laser scattering imaging, and DP-LAL (Double Pulse Laser Ablation in Liquids) for laser-induced breakdown detection. The results show that NPs are produced in the first stage of the PLAL process, i.e. during the plasma cooling. The plasma cooling starts from the external shells of the plasma and proceeds to the interior, thus the temperature in the plasma core remains constant, allowing NPs to be formed in constant thermodynamic conditions. This observation clearly explains the narrow distribution of size generally observed in NPs obtained by PLAL. Moreover, the transport and diffusion of the produced NPs in the cavitation bubble was studied with the same approach. In particular it was shown that the NPs are released in the solution during the cavitation bubble collapse phase, since the bubble itself shrinks to a smaller volume than that of the NPs cloud. The laser scattering experiments and the DP-LAL for laser-induced breakdown detection show that, as a consequence of the bubble compression during the shrinking phase, the NP cloud is concentrated in a small volume. After the bubble collapse, the NPs transfer in solution and diffuse in the liquid environment producing the colloidal solution. The study of the sequence of these processes can be useful for improving the PLAL yield and selectivity because it can allow selecting which specific stages of the overall process are most suitable for the desired NP production.

Acknowledgements:
The authors are grateful to Dr Antonio Santagata from CNR-ISM UOS PZ and Prof. Stephan Barcikowski for taking part in the scientific discussion.

References:

1. S. Barcikowski, F. Devesa, K. Moldenhauer, Impact and structure of literature on nanoparticle generation by laser ablation in liquids, J Nanopart Res (2009) 11:1883–1893
2. S. Barcikowski, G. Compagnini, Advanced nanoparticle generation and excitation by lasers in liquids, Phys. Chem. Chem. Phys., 2013, **15**, 3022-3026
3. Guowei Yang, Laser Ablation in Liquids: Principles and Applications in the Preparation of Nanomaterials, Published: February 22, 2012 by Pan Stanford
4. V. Amendola and M. Meneghetti, What controls the composition and the structure of nanomaterials generated by laser ablation in liquid solution?, Phys. Chem. Chem. Phys., 2013, 15, 3027.
5. D. Guo, G. Xie, J. Luo, Mechanical properties of nanoparticles: basics and applications, J. Phys. D: Appl. Phys. 47 (2014) 013001
6. A. De Giacomo, M. Dell'Aglio, A. Santagata, R. Gaudiuso, O.De Pascale, P. Wagener, G. C. Messina, G. Compagnini and S.Barcikowski, Cavitation dynamics of laser ablation of bulk and wire-shaped metals in water during nanoparticles production, Phys.Chem. Chem. Phys., 2013,**15**, 3083
7. M. Dell'Aglio, R. Gaudiuso, R. ElRashedy, O. De Pascale, G. Palazzo, A. De Giacomo, Collinear double pulse laser ablation in water for the production of silver nanoparticles, Phys.Chem. Chem. Phys., 2013, **15**, 20868
8. S. Ibrahimkutty, P. Wagener, A. Menzel, A. Plech, S. Barcikowsky, Nanoparticle formation in a cavitation bubble after pulsed laser ablation in liquid studied with high time resolution small angle x-ray scattering Applied Physics Letters 101 (2012) 103104.
9. P. Wagener, S. Ibrahimkutty, A. Menzel, A. Plech, S. Barcikowsky, Dynamics of silver nanoparticle formation and agglomeration inside the cavitation bubble after pulsed laser ablation in liquid. Phys, Chem. Chem. Phys. 15 (2013) 3068-3074.
10. A De Bonis, M Sansone, L D'Alessio, A Galasso, A Santagata, R Teghil, Dynamics of laser-induced bubble and nanoparticles generation during ultra-short laser ablation of Pd in liquid, J. Phys. D: Appl. Phys. 46 (2013) 445301
11. T. E. Itina, On Nanoparticle Formation by Laser Ablation in Liquids, J. Phys. Chem. C 2011, 115, 5044–5048
12. M. E. Povarnitsyn, T. E. Itina, P. R. Levashov, K. V. Khishchenko, Mechanisms of nanoparticle formation by ultra-short laser ablation of metals in liquid environment, Phys.Chem. Chem. Phys., 2013, 15, 3108

13. A. De Giacomo, A. De Bonis, M. Dell'Aglio, O. De Pascale, R. Gaudiuso, S. Orlando, A. Santagata, G. S. Senesi, F. Taccogna, and R. Teghil, Laser ablation of graphite in water in a range of pressure from 1 to 146 atm using single and double pulse techniques for the production of carbon nanostructures, J. Phys Chem. C, 2011, 115/12, 5123
14. K. Sasaki, T. Nakano, W. Soliman, N. Takada, da, Effect of pressurization on the dynamics of a cavitation bubble induced by liquid-phase laser ablation, Applied Physics Express 2 (2009) 046501
15. T. Tsuji, Y. Okazaki, Y. Tsuboi, M. Tsuji, Nanosecond Time-Resolved Observations of Laser Ablation of Silver in Water, Japanese J. Appl. Phys., 2007, 46/4, 1533
16. K. Sasaki, N. Takada, Liquid-phase laser ablation, Pure Appl. Chem., 2010, 82/6, 1317
17. Messina, P. Wagner, R. Streubel, A. De Giacomo, A. Santagata, G. Compagnini, S. Barcikowski, Pulsed laser ablation of a continuously-fed wire in liquid flow for high-yield production of silver nanoparticles, Phys. Chem. Chem. Phys. 15, 2013, 3093-3098.
18. L.J. Radziemski, D.A. Cremers (Eds.), Laser-induced plasma and applications, Marcel Dekker, New York, 1989.
19. A. De Giacomo, M. Dell'Aglio, O. De Pascale, R. Gaudiuso, V. Palleschi, C. Parigger, A. Woods, Spectrochim. Acta Part B, 100 (2014) 180-188.
20. A. Casavola, A. De Giacomo, M. Dell'Aglio, F. Taccogna, G. Colonna, O. De Pascale, S. Longo, Experimental investigation and modelling of double pulse laser induced plasma spectroscopy under water, Spectrochim. Acta part B, 60 (2005) 975-985.
21. A. De Giacomo, M. Dell'Aglio, R. Gaudiuso, S. Amoruso, O. De Pascale, Spectrochimica Acta Part B 78 (2012) 1-19.
22. H.R. Griem, Principles of Plasma Spectroscopy, Cambridge University Press, 1997
23. A. De Giacomo, M. Dell'Aglio, O. De Pascale, R. Gaudiuso, V. Palleschi, C. Parigger, A.Woods, Plasma processes and emission spectra in laser induced plasmas: A point of view, Spectrochimica Acta Part B 100 (2014) 180–188
24. A. De Giacomo, R. Gaudiuso, M. Dell'Aglio, A. Santagata, Effects of the background environment on formation, evolution and emission spectra of laser-induced plasmas, Spectrochim. Acta B 65 (2010) 385–394.
25. K. Saito, K. Takatani, T. Sakka, Y. H. Ogata, Observation of the light emitting region produced by pulsed laser irradiation to a solid–liquid interface, Applied Surface Science 197–198 (2002) 56–60

26. K. Saito, T. Sakka and Y. H. Ogata, Rotational spectra and temperature evaluation of molecules produced by pulsed laser irradiation to a graphite–water interface, J. Appl. Phys. 94, 5530 (2003).
27. C. Rehbock, J. Jakobi, L. Gamrad, S. van der Meer, D. Tiedemann, U. Taylor, W. Kues, D. Rath, S. Barcikowski, Current state of laser synthesis of metal and alloy nanoparticles as ligand-free reference materials for nano-toxicological assays, Beilstein J. Nanotechnol. 2014, *5*, 1523–1541.
28. R. Petkovsek, J. Mozina, G. Mocnik, Optodynamic characterization of the shock waves after laser induced breakdown in water, Optics Express 13/11 (2005) 4107-4112.
29. A. Vogel, S. Busch, U. Parlitz, Shock wave emission and cavitation bubble generation by picosecond and nanosecond optical breakdown in water, J. Acoust. Soc. Am. 100 (1996) 148-164.
30. O. Baghdassarian, H. C. Chu, B. Tabbert, G. A. Williams, Spectrum of Luminescence from Laser-Created Bubbles in Water, Physical Review Letters, 89 (2001) 21 4934-4937.
31. B. Wolfrum, T. Kurz, R. Mettin, W. Lauterborn, Shok wave induced interaction of microbubbles and boundaries, Physics of Fluids 15/10 (2003) 2916-2922.
32. J. Noack, D. X. Hammer, G. D. Noojin, B. A. Rockwell, A. Vogel, Influence of pulse duration on mechanical effects after laser-induced breakdown in water, J. Appl. Phys. 83/12 (1998) 7488-7495.
33. B. Ward, D. C. Emmony, Direct observation of the pressure developed in a liquid during cavitation-bubble collapse, Appl. Phys. Lett. 59, (1991) 2228-2230.
34. J. G. Fujimoto, W. Z. Lin, E. P. Ippen, C. A. Puliafito, R. F. Steinert, Time-resolved studies of Nd:YAG laser-induced breakdown. Plasma formation, acoustic wave generation, and cavitation, Invest. Ophthalmol. Vis. Sci. 26 (1985) 1771-1777.
35. P. Giovanneschi, D. Dufresne, Experimental study of laser-induced cavitation bubbles . J. Appl. Phys. 58 (1985) 651-652.
36. M. P. Felix, A. T. Ellis, Appl. Phys. Lett. Laser-Induced Liquid Breakdown-a Step-By-Step Account 19 (1971) 484-486.
37. P.K. Kennedy, D.X. Hammer, B.A. Roclwell, Prog. Quant. Electr., 1997, 21/3, 155

Table 1

t (μs)	T (K)	P (Pa)
10	609.6	2.04e+06
30	383.4	3.69e+05
50	343.9	2.34e+05
70	297.9	1.30e+05
90	343.9	1.91e+05
110	350.4	2.61e+05
130	358.4	8.41e+05
150	833.7	2.01e+07
160	913.3	5.71e+07

Table caption:

Temporal evolution of temperature and pressure values of the water vapour in the cavitation bubble as calculated with the Van der Waals equation (the bubble radius value was determined from the shadowgraphs shown in Fig. 4b). Experimental set-up is described in ref. [6].

Figure Captions:

Fig. 1: Time sequence of the processes involved during the pulsed laser ablation in liquid

Fig. 2: Shadowgraph images coupled with image taken with fast camera of laser-induced plasma and cavitation bubble on a Pt wire in water (wire diameter = 545 μm, λ_{laser}= 532 nm, irradiance = 12 GW cm^{-2} , camera gate width = 500 ns). Experimental set-up is described in ref. [6].

Fig. 3: Temporal evolution of the plasma continuum intensities and of the plasma temperatures as determined by a Planck-like distribution during ablation of Ti and Cu bulk targets immersed in water (λ_{laser} = 532 nm, irradiance = 140 GW cm^{-2}, camera gate width = 200 ns). Experimental set-up is described in ref. [6].

Fig. 4: Time-resolved shadowgraph images of the laser-induced bubble on a) a Cu wire target and b) Ti bulk target in water (λ_{laser} = 532 nm, irradiance = 12 and 34 GW cm^{-2} respectively, camera gate width = 38 and 5 μs respectively, wire diameter = 250 μm). Experimental set-up is described in ref. [6, 7].

Fig. 5: Three frames of time-resolved shadowgraph (a) and laser scattering (b) images of laser-induced bubble on a Ti bulk target and on a Cu wire target in water, respectively (λ_{laser} = 532 nm, irradiance = 12 and 34 GW cm^{-2} respectively, camera gate width = 5 μs, wire diameter = 250 μm). Experimental set-up is described in ref. [6].

Fig. 6: A schematic behaviour of the bubble volume and the NPs cloud during the different stages of the bubble lifetime: r and R are the bubble and the NPs cloud radii, respectively.

Fig. 7: a) Shadowgraph images of bubble and plasma induced by P-PLAL on an Ag bulk target in water at different interpulse delays (and with different camera gate width): the images show the plasma induced by the second laser pulse inside the bubble induced by the first laser pulse, at different moments during the bubble lifetime. b) The temporal evolution of the laser-induced bubble radius as measured from shadowgraph images during a single-pulse LAL experiment is reported by comparison. (λ_{laser} = 532 nm, irradiance = 17.5 GW cm^{-2}, gate width is reported on each frame). Experimental set-up is described in ref. [7].

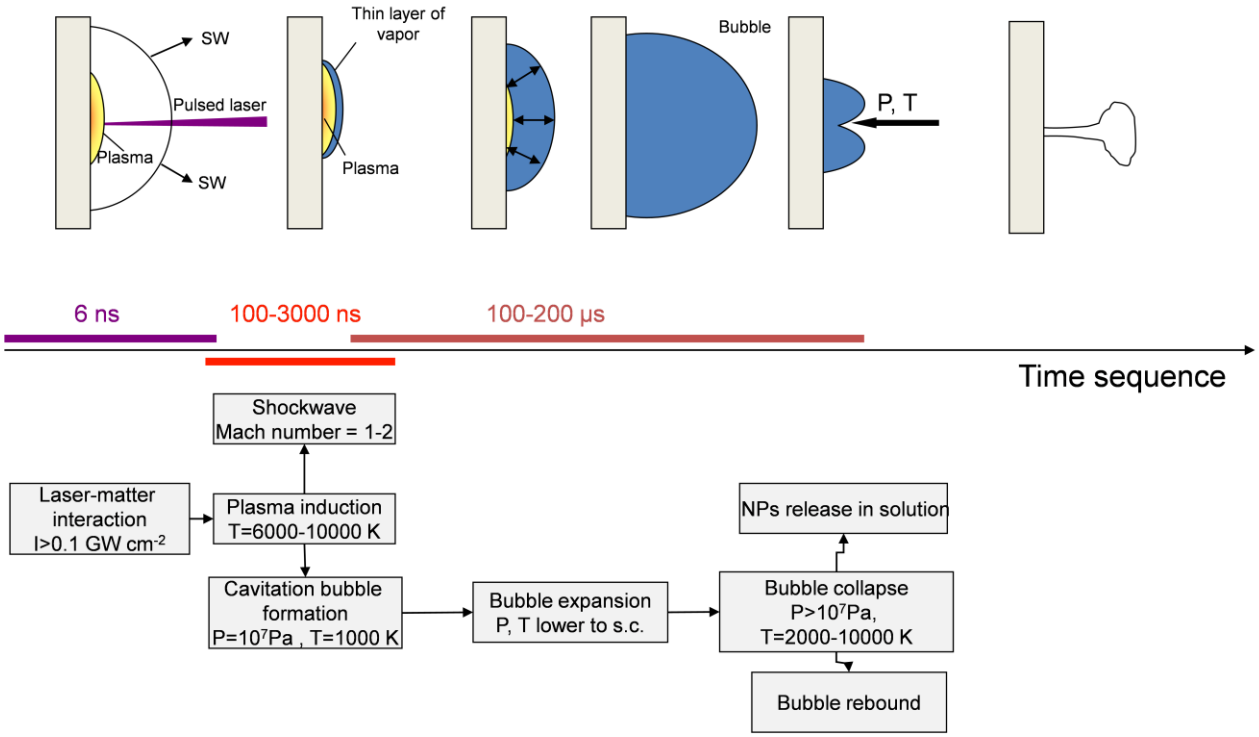
SW
Pulsed laser
Plasma
SW
Thin layer of vapor
Plasma
Bubble
P, T
6 ns
100-3000 ns
100-200 µs
Time sequence
Shockwave
Mach number = 1-2
Laser-matter interaction
I>0.1 GW cm-2
Plasma induction
T=6000-10000 K
Cavitation bubble formation
P=10^7Pa , T=1000 K
Bubble expansion
P, T lower to s.c.
Bubble collapse
P>10^7Pa,
T=2000-10000 K
NPs release in solution
Bubble rebound

Fig. 1

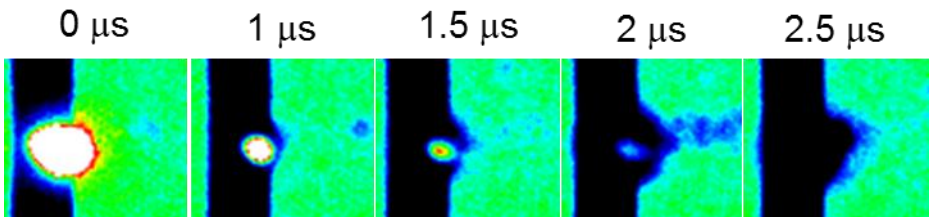

Fig. 2

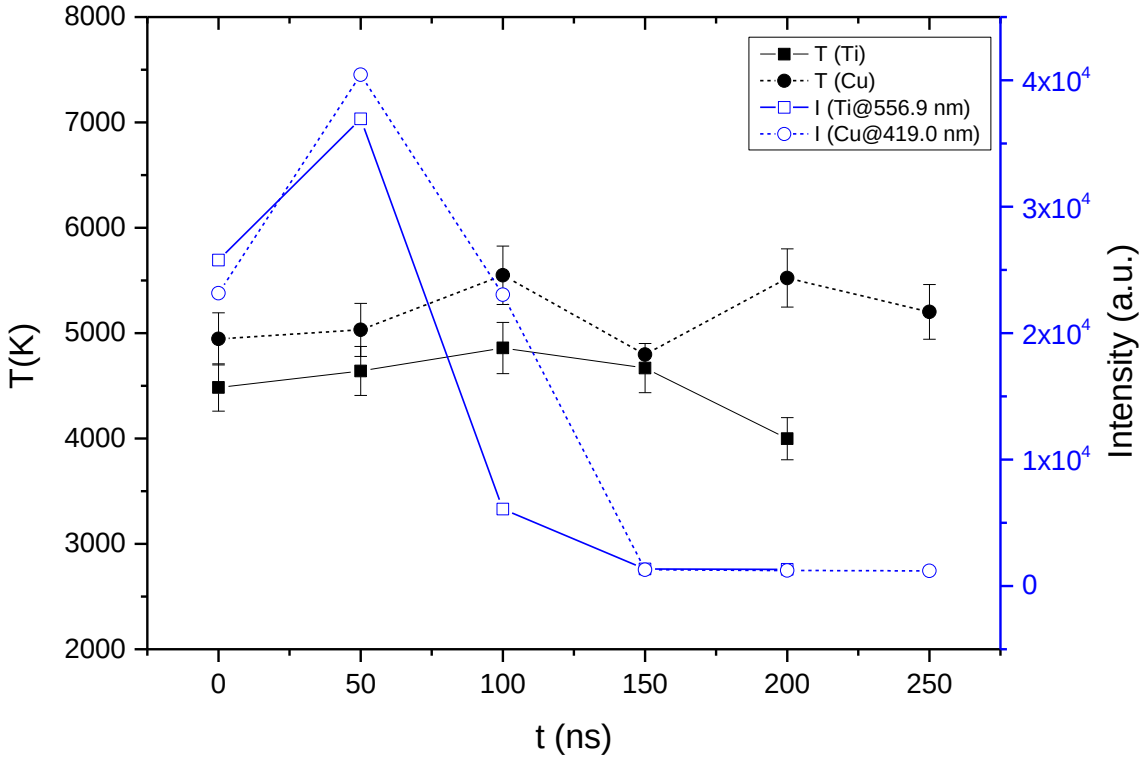
T (Ti)
T (Cu)
I (Ti@556.9 nm)
I (Cu@419.0 nm)
T(K)
Intensity (a.u.)
t (ns)
8000
7000
6000
5000
4000
3000
2000
0
50
100
150
200
250
4x10^4
3x10^4
2x10^4
1x10^4
0

Fig. 3

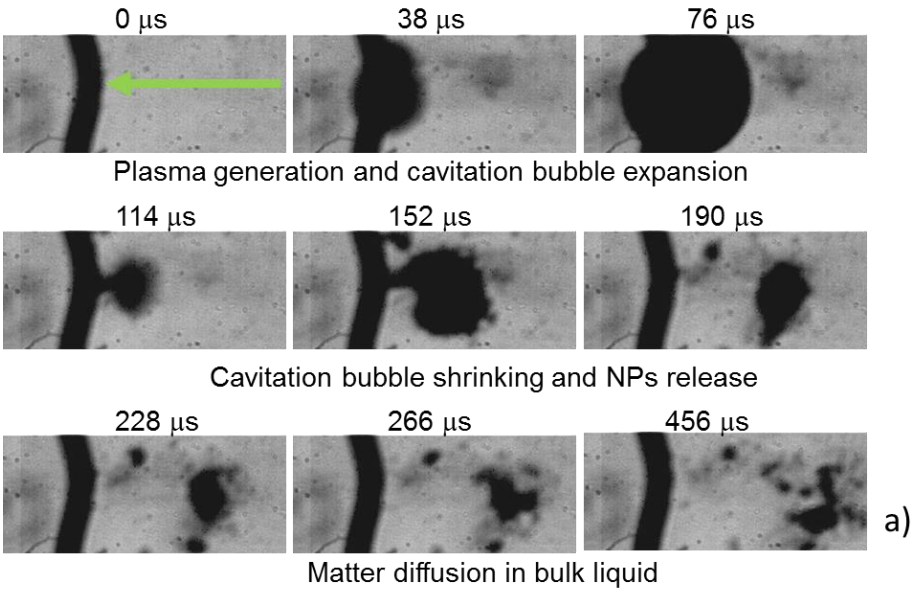
0 µs
38 µs
76 µs
Plasma generation and cavitation bubble expansion
114 µs
152 µs
190 µs
Cavitation bubble shrinking and NPs release
228 µs
266 µs
456 µs
Matter diffusion in bulk liquid
a)

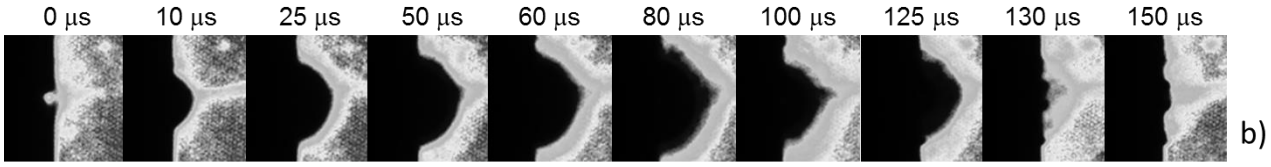
0 µs
10 µs
25 µs
50 µs
60 µs
80 µs
100 µs
125 µs
130 µs
150 µs
b)

Fig. 4

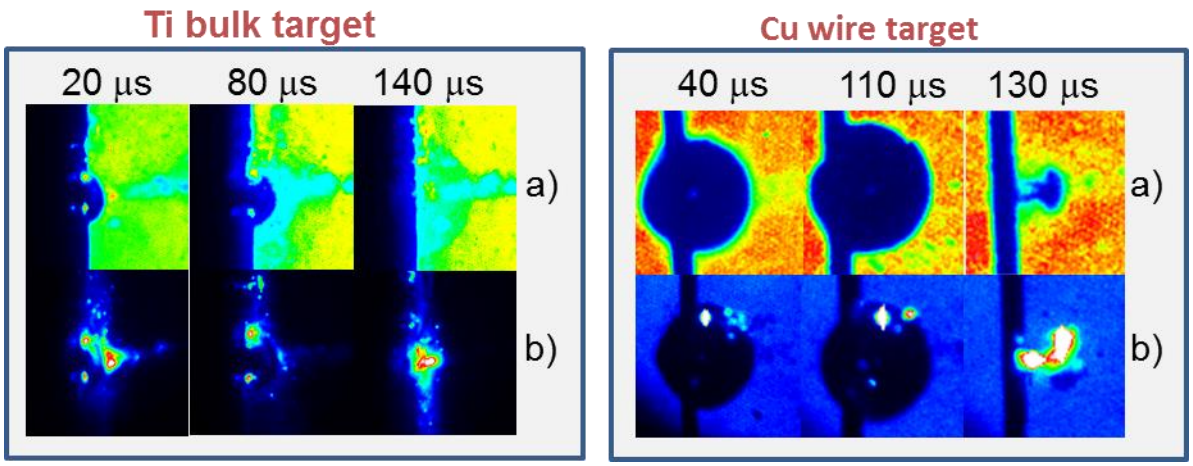
Ti bulk target
20 μs
80 μs
140 μs
a)
b)
Cu wire target
40 μs
110 μs
130 μs
a)
b)

Fig. 5

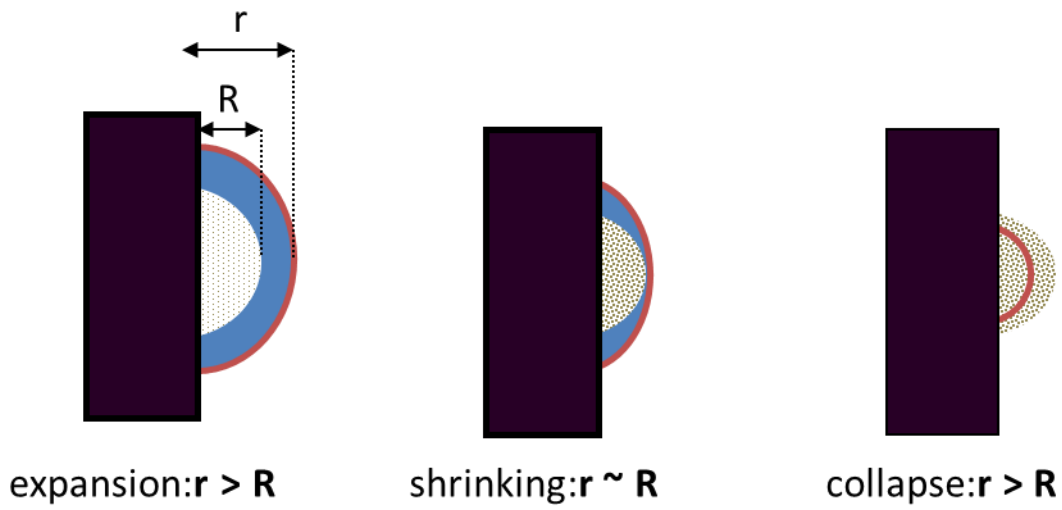

Fig. 6

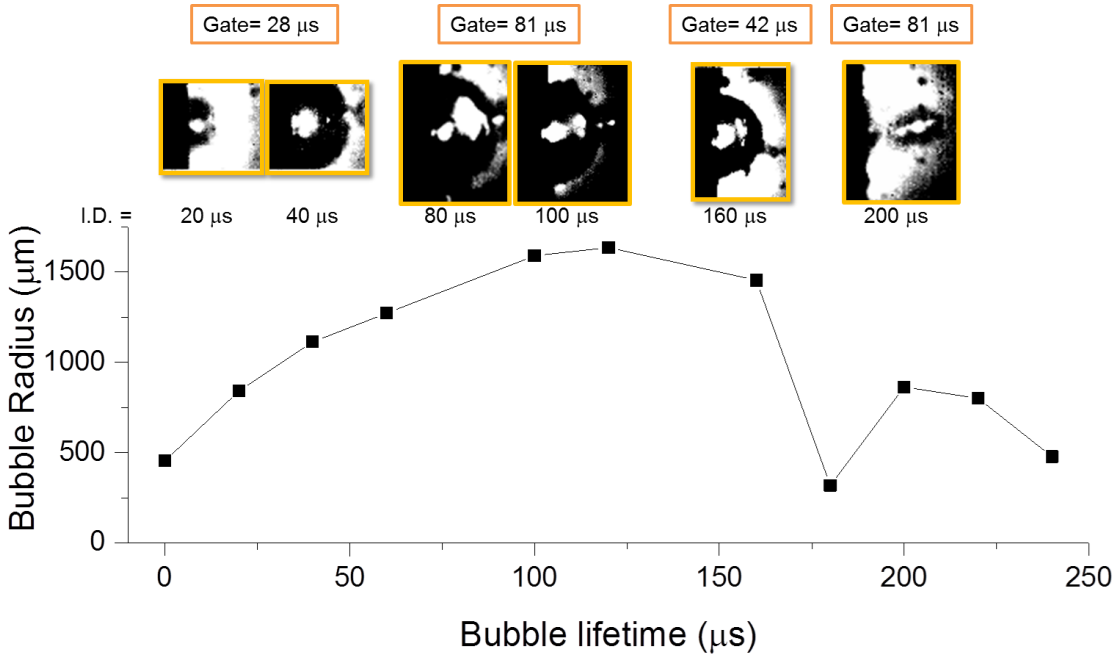
Gate= 28 µs
Gate= 81 µs
Gate= 42 µs
Gate= 81 µs
I.D. =
20 µs
40 µs
80 µs
100 µs
160 µs
200 µs
Bubble Radius (µm)
0
500
1000
1500
0
50
100
150
200
250
Bubble lifetime (µs)

Fig. 7